scientific reports

Check for updates

OPEN

Black-necked spitting cobra (*Naja nigricollis*) phospholipases A_2 may cause *Trypanosoma brucei* death by blocking endocytosis through the flagellar pocket

Andrea Martos-Esteban[1], Olivia J. S. Macleod[1], Isabella Maudlin[1], Konstantinos Kalogeropoulos[2], Jonas A. Jürgensen[2], Mark Carrington[1] & Andreas H. Laustsen[2]✉

African trypanosomes, such as *Trypanosoma brucei*, are flagellated protozoa which proliferate in mammals and cause a variety of diseases in people and animals. In a mammalian host, the external face of the African trypanosome plasma membrane is covered by a densely packed coat formed of variant surface glycoprotein (VSG), which counteracts the host's adaptive immune response by antigenic variation. The VSG is attached to the external face of the plasma membrane by covalent attachment of the C-terminus to glycosylphosphatidylinositol. As the trypanosome grows, newly synthesised VSG is added to the plasma membrane by vesicle fusion to the flagellar pocket, the sole location of exo- and endocytosis. Snake venoms contain dozens of components, including proteases and phospholipases A_2. Here, we investigated the effect of *Naja nigricollis* venom on *T. brucei* with the aim of describing the response of the trypanosome to hydrolytic attack on the VSG. We found no evidence for VSG hydrolysis, however, *N. nigricollis* venom caused: (i) an enlargement of the flagellar pocket, (ii) the Rab11 positive endosomal compartments to adopt an abnormal dispersed localisation, and (iii) cell cycle arrest prior to cytokinesis. Our results indicate that a single protein family, the phospholipases A_2 present in *N. nigricollis* venom, may be necessary and sufficient for the effects. This study provides new molecular insight into *T. brucei* biology and possibly describes mechanisms that could be exploited for *T. brucei* targeting.

African trypanosomes are protozoan pathogens that have evolved the capacity to evade the mammalian innate and adaptive immune systems, and infection causes a variety of diseases in people and livestock[1]. In a mammalian host, the external face of the *Trypanosoma brucei* plasma membrane is covered by a densely packed coat formed by variant surface glycoprotein (VSG)[2]. VSG is at the centre of a population survival strategy based on antigenic variation, enabling the infection to avoid clearance by the host's adaptive immune response (Fig. 1A). The VSG is also central to individual cell survival strategy: Once an immunoglobulin (Ig) binds a VSG, the complex (VSG-Ig) protrudes above the surface coat and is subject to hydrodynamic forces, imposed by the swimming motion of the cell, causing the VSG-Ig to move towards the cell posterior pole and the flagellar pocket where it is endocytosed[3,4]. The flagellar pocket is an invagination within the plasma membrane[5], from where the flagellum exits the cell body and is the sole site of endo- and exocytosis[3] (Fig. 1B). The rate of endocytosis is particularly high in trypanosomes[6,7], and is all clathrin-mediated[8]. After endocytosis, Ig is trafficked through the internal endocytic pathway to the lysosome. This movement of cargo occurs through compartments that are highly polarised along an axis from the flagellar pocket to the lysosome, which lies close to the nucleus (Fig. 1C)[9,10].

Snake and bee toxins have been used as tools for the study of trypanosomatid-related diseases. In particular, several studies have shown the effect of various phospholipases A_2 in trypanosomatids. Phospholipase A_2 (PLA_2) present in *Apis mellifera* is lethal to *T. brucei*[11]; PLA_2 BnSP-7 from *Bothrops pauloensis*[12] and Asp49- and Lys49-PLA_2s from *Bothrops mattogrossensis*[13] interfere with proliferation and infectivity of *Leishmania amazonensis*.

[1]Department of Biochemistry, University of Cambridge, Cambridge CB2 1QW, UK. [2]Department of Biotechnology and Biomedicine, Technical University of Denmark, Kongens Lyngby, Denmark. ✉email: ahola@bio.dtu.dk

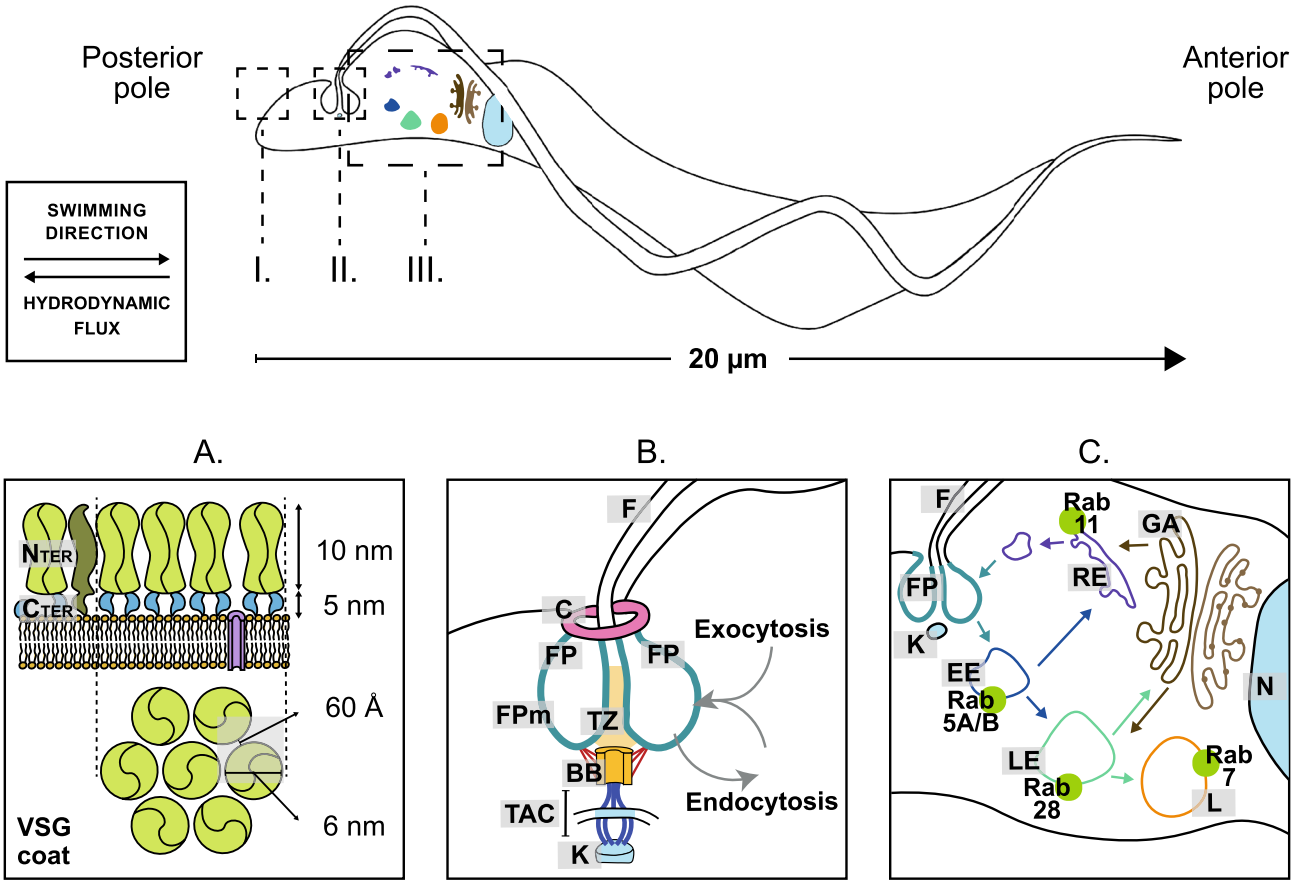

Figure 1. *T. brucei* morphology: (**A**) VSG coat structure. The plasma membrane is covered by a densely packed VSG coat. VSG constitutes over 95% of the surface coat components[2]. (**B**) Flagellar pocket structure[5]. The flagellar pocket (FP) is the sole site of endo- and exocytosis. This invagination is structured by a highly specialised membrane (FPm) penetrated by the flagellum (F) and stabilised by the flagellar pocket collar (C). The flagellum is attached to the cell body by the basal body (BB), which is connected by the tripartite attachment zone to the kinetoplast (K), the kinetoplastids' unique organelle. (**C**) Endocytosis and exocytosis pathways in *T. brucei*[2,3]. Cargo is endocytosed in the flagellar pocket. The invaginated vesicles fuse to the Rab5A/B + early endosome (EE). Then, cargo can be sent for recycling or for modification/degradation. Via the recycling pathway, cargo goes to the Rab11 + recycling endosome (RE), and finally is exocytosed through the flagellar pocket. Should the cargo undergo modification/degradation, it is sent to the Rab28 + late endosome (LE). There, cargo is sent either for degradation via Rab7 + lysosome (L) or for modification via the Golgi apparatus (GA).

In general, PLA_2s from a range of venoms have a sequence identity of 40% to 99% and a conserved structure, with a four alpha-helix core, where each helix is joined by a loop or a sheet[14]. Despite sequence and structural homology, different subtypes of PLA_2s have been shown to play diverse functions and mechanisms of action[15,16]. However, the molecular pathways triggering trypanocidal effects and phenotypes that are likely caused by PLA_2s have not been investigated.

Naja nigricollis (the black-necked spitting cobra) is one of the medically most important snakes found across West, Central, and East Africa[17]. It is known for having a venom rich in PLA_2s and cytotoxic three-finger toxins that combined cause severe cytotoxicity, manifesting as local tissue damage and necrosis in mammalian victims. Here, we investigate the effects of *N. nigricollis* venom (NNV) on *T. brucei* at the mechanistic and molecular level. We show that NNV is trypanocidal and identify the lethal components to likely be PLA_2s, which comprise ~ 22% of total venom protein[17]. We show that the PLA_2s present in NNV are likely the first external effector causing massive flagellar pocket enlargement, the 'Big Eye' phenotype[8]. This phenotype was first described in trypanosomes in which clathrin light chain[8] or actin[18] had been depleted, and enlargement of the flagellar pocket occurs as membrane is still added by exocytosis, but none removed by endocytosis, eventually resulting in cell death.

Results

***N. nigricollis* venom causes *T. brucei* cell death.** To assay for potential effects on the growth rate and survival, cultures of *T. brucei* were incubated with NNV over 24 h (Fig. 2A). By comparison to a no treatment control, 5 µg/mL NNV was the minimum effective concentration able to kill the trypanosome population within 24 h, whereas 20 µg/mL NNV caused cell death within 8 h. At the end of the time course, no cells were left in culture as a result of cell lysis.

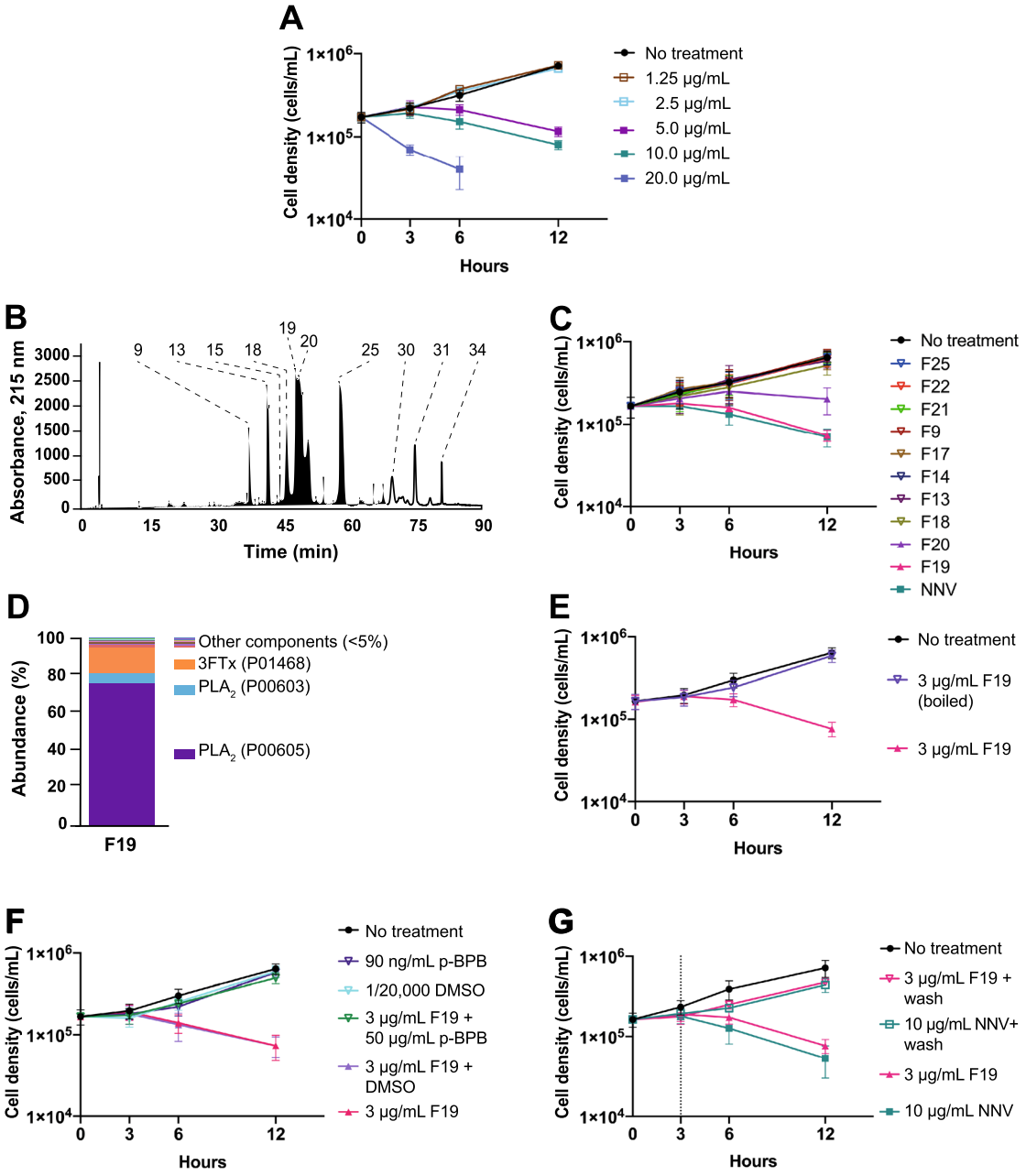

Figure 2. *N. nigricollis* PLA_2s seem to be the necessary and sufficient venom components to induce trypanocidal activity. (**A**) *N. nigricollis* venom (NNV) causes rapid *T. brucei* death. 20 µg/mL NNV kills the entire population of *T. brucei* within 8 h. 5 µg/mL NNV was the minimum effective concentration able to kill the cell population within 24 h. (**B**) NNV chromatogram. NNV was fractionated by RP-HPLC. (**C**) Fractions containing PLA_2s retain trypanocidal activity, showing that PLA_2s are likely the necessary components to induce cell death. Fraction 19 containing PLA_2s and the juxtaposed fraction 20, also containing PLA_2s, retained trypanocidal activity upon venom fractionation. Venom fractions were tested at 3 µg/mL. NNV was tested at 10 µg/mL. (**D**) Fractions retaining lethal effects contain PLA_2s. LC–MS analysis of fraction 19. The relative abundance of PLA_2s in fraction 19 is 83%. (**E**) PLA_2s require tertiary structure to exert their observed trypanocidal activity. 3 µg/mL. Fraction 19 was incubated at 100 °C for 5 min and then further incubated for 12 h with cultures of *T. brucei* VSG121 wild type. Boiled fraction 19 imperiled trypanocidal activity. (**F**) PLA_2s require their intact catalytic activity to exert trypanocidal activity. Fraction 19 was incubated for 1 h at room temperature with 50 µg/mL *p*-bromophenacyl bromide (*p*-BPB), and further incubated with *T. brucei* cultures. for 12 h. Chemical modification of the PLA_2s catalytic His-47 rescued cell growth. (**G**) PLA_2 action seems sufficient to induce trypanocidal activity. Cultures of *T. brucei* VSG121 wild type were incubated with 3 µg/mL fraction 19 for 3 h. Then, cells were washed in fresh HMI-9 media. Finally, cells were resuspended in further 10 mL HMI-9 media and incubated up to 12 h. Cells recover upon media replacement, confirming the trypanocidal activity is caused by fraction 19 in a time-dependent manner (N = 3).

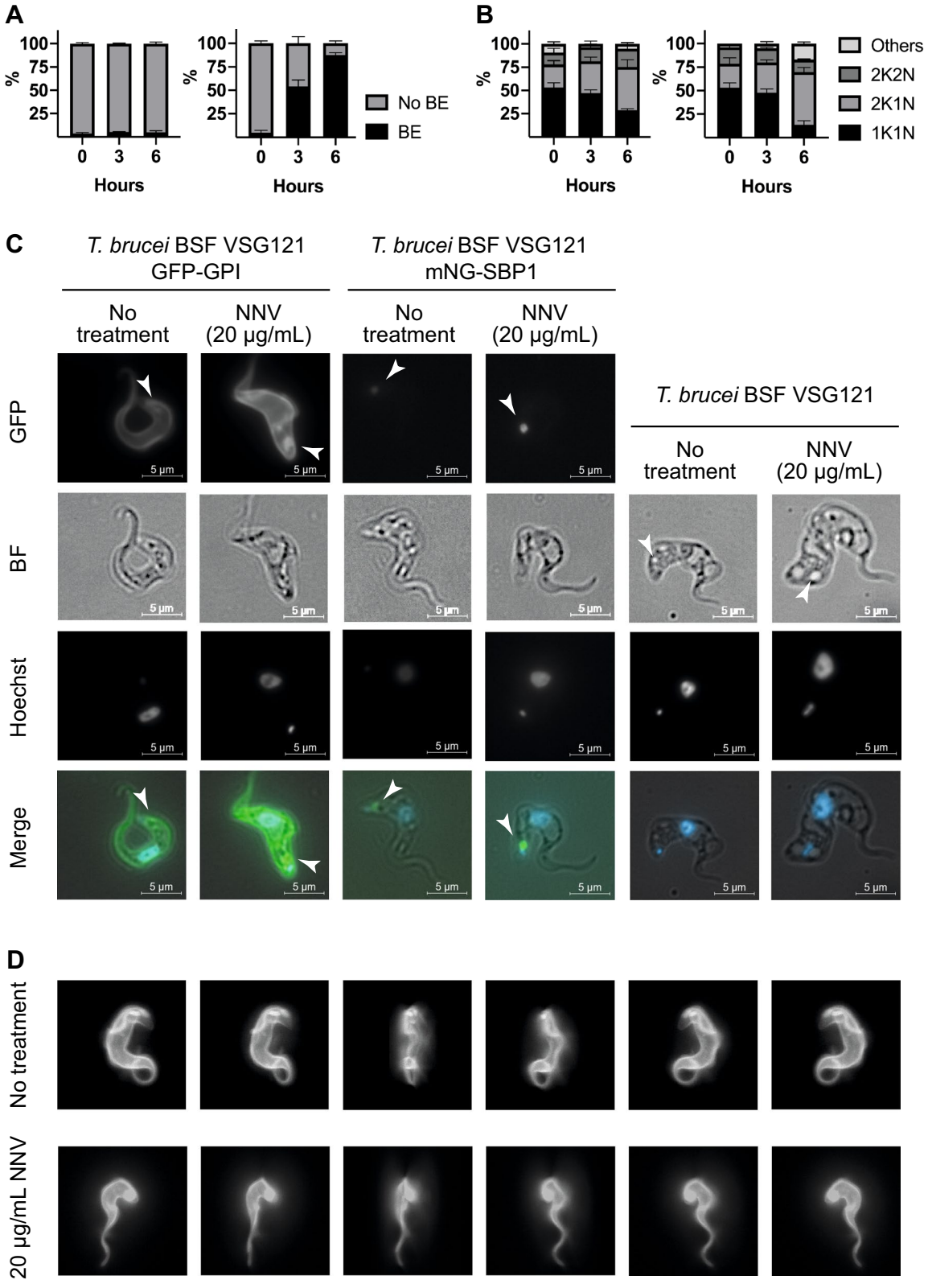
A
100
75
50
25
%
0 3 6
Hours
No BE
BE
B
Others
2K2N
2K1N
1K1N
C
T. brucei BSF VSG121 GFP-GPI
T. brucei BSF VSG121 mNG-SBP1
T. brucei BSF VSG121
No treatment
NNV (20 µg/mL)
GFP
BF
Hoechst
Merge
5 µm
D
No treatment
20 µg/mL NNV

◂**Figure 3.** PLA_2s seem to be the cause for the enlargement of the flagellar pocket. (**A**) PLA_2s cause Big Eye phenotype on *T. brucei*. Cultures of *T. brucei* VSG121 GFP-GPI were incubated with 20 µg/mL NNV, and the absence or presence of Big Eye phenotype (BE) was recorded for 300 cells (N = 3). Left graph, no treatment; right graph, 20 µg/mL NNV. At 3 h post-NNV addition, over 50% of the cells present BE. 6 h post-NNV addition, over 85% cells display BE. (**B**) PLA_2s likely compromise cell cycle progression. Cultures of *T. brucei* VSG121 wild type were incubated with 20 µg/mL NNV. Samples were taken at 0, 3, and 6 h post-NNV addition. The cell cycle stage (1K1N, 2K1N, 2K2N, other) was annotated for 300 cells (N = 3). Left graph, no treatment, right graph, 20 µg/mL NNV. A 25% increase of 2K1N cells and a fourfold increase of cells fitting within the 'other' category (i.e. cell cycle abnormalities) were observed as a consequence of the PLA_2 effect. These observations indicate that cells try to progress through the cell cycle up to the duplication of the kinetoplast, and then they cannot proceed any further. (**C**) SBP1-mNG distribution indicated an expansion of the flagellar pocket membrane. Fixed fluorescence microscopy was performed prior to NNV addition and 6 h post-NNV addition to *T. brucei* BSF VSG121 GFP-GPI, *T. brucei* BSF VSG121 SBP1-mNG, and *T. brucei* BSF VSG121. Accumulation occurs at the flagellar pocket, as it can be observed in the GFP panels. Accumulation is not a by-product of GFP or mNG expression, as it can be observed in DIC images for wild type cells as well as in the modified cell lines. (**D**) Accumulation occurs at the flagellar pocket membrane, not passively at the empty space created by the flagellar pocket membrane. Fixed confocal fluorescent microscopy was used to create 3D reconstructions of the cells with and without NNV (6 h post-addition). The panels represent snapshots of the 3D reconstructed cell rotating over itself so every angle is visible (top row panels, no treatment; bottom row panels NNV treatment).

***N. nigricollis* PLA_2s are likely necessary and sufficient to induce trypanocidal activity.** To elucidate which of the venom components were responsible for *T. brucei* cell death, NNV was fractionated by reversed-phase HPLC (Fig. 2B) and individual fractions were tested for trypanocidal activity. Cultures of *T. brucei* were incubated for 24 h with fractions 9, 13, 15, 18, 19, 20, 21, 25, 30, 31, and 34 as these contained the most abundant venom proteins (Fig. 2C). Growth was compared to no treatment and NNV (10 µg/mL) controls. In one set of growth assays, fractions were tested at 3 µg/mL protein, corresponding to the maximum relative abundance of a known single fraction (Fig. 2C). Fraction 19 killed trypanosomes with the same potency and in a similar timeframe compared with NNV. Fraction 20 slowed down growth rate but was not as effective as fraction 19. No other fraction affected cell survival or growth rate at the tested concentrations.

Fraction 19 was then characterised by LC–MS to analyse its composition in full (Fig. 2D). LC–MS analysis found 150 peptide groups from 10,256 peptide spectrum matches, belonging to 33 master protein groups. Out of these, 12 were identified with two or more unique peptides. Label free quantification showed two phospholipase A_2 species (UniProt codes: P00605 and P00603), and one cytotoxin (UniProt code P01468) being the most abundant proteins in the fraction. In total, quantification indicated that phospholipase A_2 proteoforms accounted for approximately 83% of the protein content in the fraction, followed by cytotoxins at 15%.

We proceeded to investigate the role of PLA_2s in trypanosome cell death. PLA_2s were inactivated by two methods. First, fraction 19 was incubated at 100 °C for 5 min prior to incubation at 3 µg/mL with cultures of *T. brucei* for 24 h (Fig. 2E). The growth was measured and compared to no treatment and native fraction 19 controls. After heat treatment, fraction 19 had no effect on cell proliferation. Second, fraction 19 was incubated with 50 µg/mL *p*-bromophenacyl bromide (*p*-BPB), an inhibitor for PLA_2s that covalently binds the catalytic histidine 47[19]. (Fig. 2F). Cell proliferation was measured and compared to a set of controls: (i) no treatment; (ii) *p*-BPB; (iii) DMSO (*p*-BPB solvent); (iv) DMSO + fraction 19; and (v) fraction 19. When Fraction 19 was incubated with *p*-BPB, it did not interfere with cell proliferation, indicating that the trypanocidal activity of the PLA_2s was lost through selective inhibition. Third, cultures of *T. brucei* were incubated with fraction 19 for 3 h (Fig. 2G). Then, cells were washed in fresh HMI-9 media and resuspended in further 10 mL HMI-9 media. Last, cells were incubated for an extra 5 h. Cell proliferation was measured and compared to a set of controls: (i) no treatment and (ii) no-washing in fresh media. Cell proliferation was recovered upon removal of media containing PLA_2s. These observations indicate that PLA_2s were the necessary and sufficient NNV component to induce trypanosome cell death.

The enlargement of the flagellar pocket is likely induced by PLA_2s. Upon observation that PLA_2s are likely to be the components causing cell death, changes in cell morphology over a time course after addition of PLA_2s were investigated. Initial experiments were designed to investigate potential PLA_2 effects on the cell surface. A *T. brucei* cell line expressing a cell surface GPI-anchored enhanced GFP (eGFP) in a VSG121 background was used to visualise the cell surface coat. Cultures of *T. brucei* BSF VSG121 GFP-GPI were incubated with 20 µg/mL NNV for 6 h (Fig. 3A). Cell morphology was recorded prior to NNV addition, 3 h and 6 h post-NNV addition, and compared to no treatment conditions. At 3 h post-NNV addition, around 50% of the trypanosomes had an enlarged flagellar pocket similar to the 'Big Eye' phenotype caused by blocking of endocytosis. At 6 h, over 80% of the cells displayed the Big Eye phenotype.

In a second set of experiments, the effect of NNV on the cell cycle was analysed (Fig. 3B). This experiment was carried out in the same conditions as the first, except wild type VSG121 expressing cells were used and Hoechst 33342 was used to visualise the nucleus and kinetoplast. At 6 h post-NNV addition, a 25% increase in cells with 2 kinetoplasts (2K1N) was observed when compared to no treatment conditions. In addition, a fourfold increase in cells presenting a range of cell cycle abnormalities was observed, such as incomplete cell division resulting in two daughter cells remaining joined by the posterior ends and cells with only one kinetoplast but two nuclei.

The effect on the flagellar pocket was investigated further by making a cell line with one endogenous allele of syntaxin binding protein 1 (SBP1, Tb927.9.1970) tagged at the C-terminus with mNeon Green fluorescent protein

(mNG)[20] as a flagellar pocket membrane marker[21,22]. Cultures of *T. brucei* BSF VSG121 expressing SBP1-mNG were incubated with 20 µg/mL NNV for 8 h. Cell morphology was analysed by fluorescence microscopy prior to NNV addition and 6 h post-NNV addition, and compared to no treatment conditions. *T. brucei* BSF VSG121 GFP-GPI and *T. brucei* BSF VSG121 wild type were treated in parallel (Fig. 3C). The flagellar pocket in the SBP1-mNG expressing cells was enlarged, indicating that *N. nigricollis* PLA_2s disrupt normal flagellar pocket function.

To further characterise the nature of the accumulation causing an enlarged flagellar pocket, confocal microscopy was performed on *T. brucei* BSF VSG121 GFP-GPI cells 6 h after 20 µg/mL NNV addition and compared to no treatment control (Fig. 3D). The flagellar pocket in NNV-treated cells adopts a sphere-like shape, and the accumulation of GFP-GPI is located at the membrane, as opposed to being released from the flagellar pocket membrane and endocytosed.

The toxic effect causes arrest of endocytosis, likely mediated by PLA_2s. The next set of experiments investigated the nature and origin of the flagellar pocket enlargement. First, membrane accumulation could be the result of newly synthesised plasma membrane being exported to the flagellar pocket but not released onto the cell body. Alternatively, enlargement could result from an inhibition of endocytosis. To distinguish between these two possibilities, protein translation was inhibited using cycloheximide (CHX) prior to addition of NNV[23].

First, cultures of *T. brucei* BSF VSG121 wild type were incubated with 50 µg/mL CHX for 1 h, and then 20 µg/mL NNV was added. Cells were incubated for a total of 9 h. Cell growth was measured prior to CHX addition and 1, 4, and 7 h post CHX addition. A set of controls was carried out in parallel: (i) no treatment; (ii) 50 µg/mL CHX, and (iii) 20 µg/mL NNV. As expected, CHX slowed down the growth rate (Fig. 4A). The growth rate in the culture incubated with NNV and CHX was less slowed down than in those with only NNV. The effect of CHX, although statistically minor, it is still observable. The implications of this observation are discussed in the following section.

In a second set of experiments, *T. brucei* BSF VSG121 SBP1-mNG cells were incubated with 50 µg/mL CHX for 1 h, and then 20 µg/mL NNV was added. Cell morphology was analysed at 4 h and 7 h after CHX addition. A set of control conditions were carried out in parallel: (i) no treatment and (ii) 20 µg/mL NNV (Fig. 4B). The proportion of cells with an enlarged flagellar pocket caused by NNV was similar with and without CHX. This observation implied that flagellar pocket enlargement more likely occurred due to inhibition of endocytosis.

T. brucei BSF VSG121 wild type and *T. brucei* BSF VSG121 GFP-GPI treated as above were imaged by fluorescence microscopy (Fig. 4C). As described before, regardless of protein synthesis inhibition, the enlarged flagellar pocket persisted throughout the tested cell lines. No morphological effect was detected on cells treated with CHX only, but trypanosomes died within 24 h.

Last, a third set of experiments was carried out to confirm that endocytosis is the cellular process inhibited by the toxic components. To investigate this, an AF-568-transferrin uptake assay was performed. *T. brucei* BSF VSG121 GFP-GPI cells were incubated for 8 h with 20 µg/mL NNV. At 0, 0.5, 1.5, and 6 h, sample aliquots were taken. The cells were washed and resuspended in fresh HMI-9 media without serum, and FMK24 was added to inhibit lysosome function[24] in order to enable lysosomal accumulation, and thus visualization, of AF-568-transferrin. Then, the cells were incubated with AF-568-transferrin for 1 h to allow for endocytosis. Last, the cells were visualised by fluorescent microscopy. A no treatment control was carried out in parallel. (Fig. 4D,E). Cells treated with NNV did not show AF-568 transferrin uptake beyond 1.5 h after treatment onset. Non-treated cells could endocytose AF-568-transferrin consistently throughout the time course.

The flagellar pocket is the primary target for the toxic effects likely caused by PLA_2s. In the experiments above, PLA_2 treatment seemed to cause a reduced density of GFP-GPI on the plasma membrane covering the cell body. We investigated whether this decrease represents a loss of GPI-anchored proteins, possibly due to PLA_2 action (Fig. 5A), or a redistribution to the flagellar pocket. Cultures of *T. brucei* BSF VSG121 wild type, VSG121 GFP-GPI, and VSG121 SBP1-mNG were incubated with 20 µg/mL NNV with or without one hour pretreatment with CHX, and samples were analysed by flow cytometry prior to NNV addition and 6 h post-NNV addition (Fig. 5B). The total cell fluorescence was unchanged, except for a slight decrease in the double treatment group. This observation indicates there is a redistribution of cell surface proteins to the flagellar pocket rather than a loss.

PLA_2s likely compromise Rab11-mediated recycling pathway fitness. To evaluate whether other subcellular compartments involved in endo- and exocytosis are affected by NNV, a set of cell lines with different mNG-tagged subcellular compartments were used. Rab5A (*T. brucei* BSF VSG121 mNG-Rab5A) and Rab5B (*T. brucei* BSF VSG121 mNG-Rab5B) were tagged for the early endosome, Rab7 (*T. brucei* BSF VSG121 mNG-Rab7) for the late endosome, and Rab11 (*T. brucei* BSF VSG121 mNG-Rab5A) for the recycling endosome. Cultures of these *T. brucei* cell lines were incubated with 20 µg/mL NNV and imaged by fluorescence microscopy 6 h after NNV addition (Fig. 6). No observable effect was found in the early endosome (Rab5A and Rab5B) or late endosome (Rab7). In contrast, a slight distortion of the Rab11 wild type pattern was caused by NNV. Rab11 appeared in a more dispersed pattern, as opposed to the no treatment control, where Rab11 was located in discrete spots. This observation indicates that the recycling route is affected by PLA_2 activity.

Discussion

In the mammalian bloodstream, the trypanosome cell surface is covered by a densely packed coat of VSG molecules. As individual bloodstream form trypanosomes grow, newly synthesised VSG-coated plasma membrane is added to the existing plasma membrane. At the same time, pre-existing VSG-coated plasma membrane is

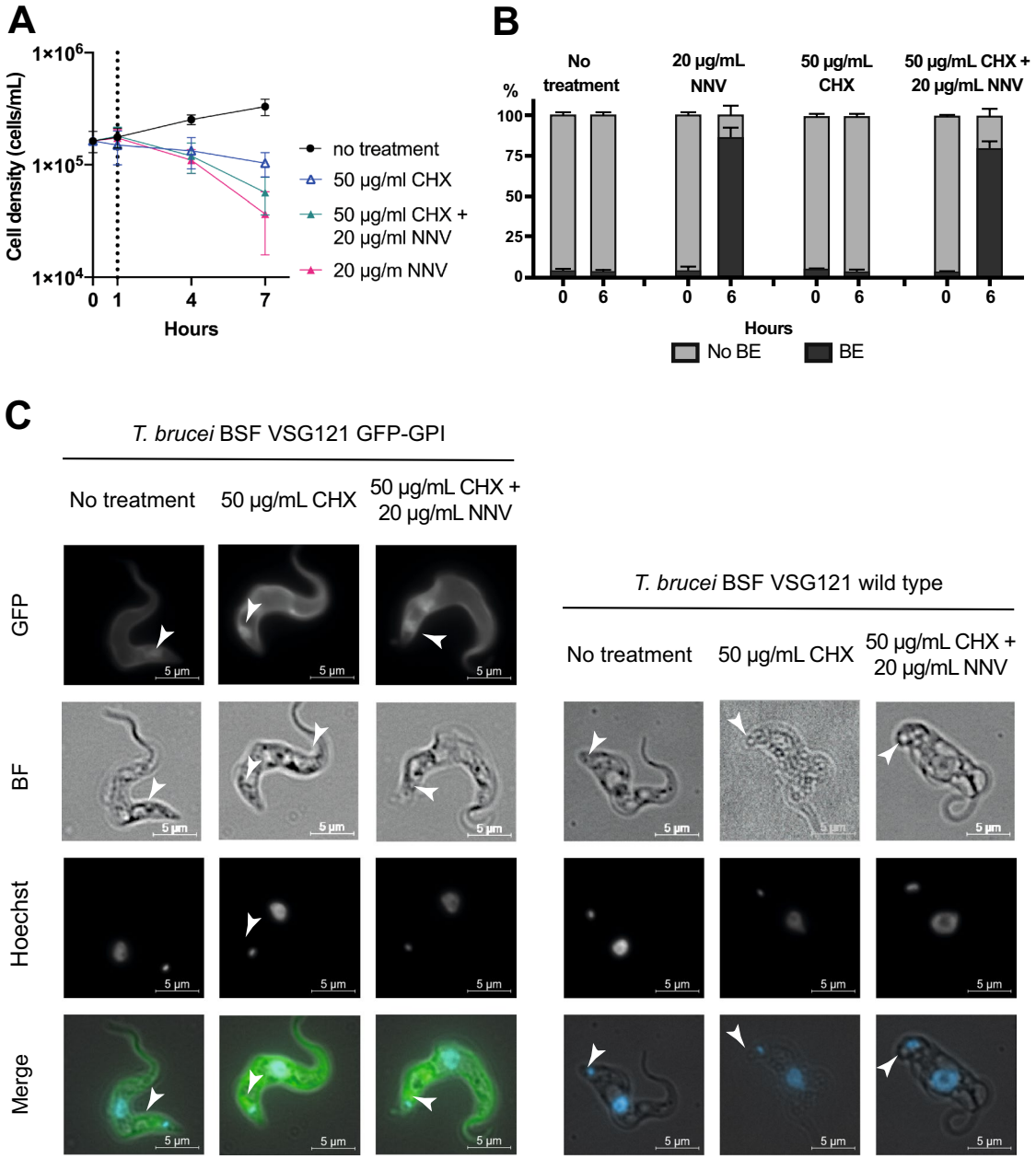

Figure 4. PLA_2s seems to inhibit endocytosis of *T. brucei* plasma membrane components at the site of the flagellar pocket. (**A**) Protein synthesis inhibition lessens the cell growth phenotype caused by PLA_2 toxicity. Cells were incubated with cycloheximide (CHX), NNV, or both, and cell growth was monitored. *T. brucei* BSF VSG121 wild type cells incubated with CHX/NNV die more slowly than those cells incubated with NNV only. (**B**) CHX reduces the proportion of cells presenting Big Eye phenotype (BE), likely caused by the action of PLA_2s, by 15–25%. *T. brucei* BSF VSG121 GFP-GPI cells were incubated with identical conditions as in (**A**), and the absence or presence of BE in 300 cells (N = 3) was annotated utilising live fluorescence microscopy. (**C**) Blockade of inside-out cargo trafficking relieves BE phenotype intensity. Fixed fluorescence microscopy was performed at 3 and 6 h post-NNV addition (equivalent to 4 and 7 h post CHX addition) on *T. brucei* BSF VSG121 wild type and *T. brucei* BSF VSG121 GFP-GPI. A milder (i.e. smaller) BE phenotype could be observed when cells were treated with CHX/NNV, indicating that the PLA_2 blockade effect occurs at the endocytosis pathway. (**D**) AF-568-transferrin uptake assay demonstrates that endocytosis is the cellular process that is inhibited by the toxic components. Top panel, non-treated control. Bottom panel, cells were treated with 20 µg/mL NNV, and AF-568-transferrin uptake was analysed. No uptake was observed beyond 1.5 h after treatment onset. Panels are representative of 95–98% of the cells observed (3 × 100 cells analysed per treatment condition).

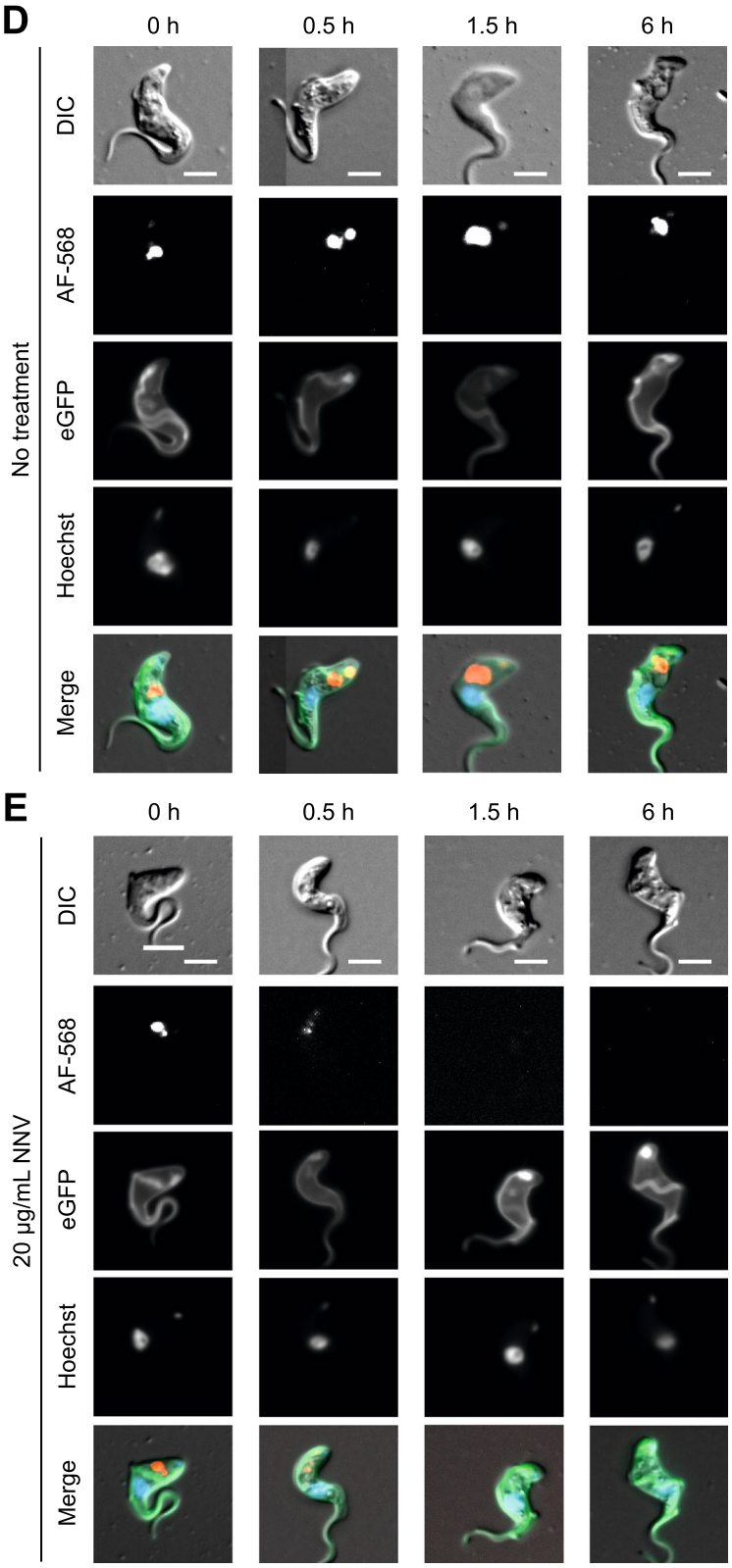

Figure 4. (continued)

endocytosed from the flagellar pocket and returned after a circular digression around the endosomal system. The processes of biogenesis, exocytosis, endocytosis, and recycling of VSG molecules are pivotal to trypanosome survival[25], as VSG represents over 10% of the total protein content and more than 90% of surface proteins. Remarkably, trypanosomes have the ability to recycle the entire surface coat within 12 min[7]. The flux of recycling VSG is at least 10 times greater than the flux of newly synthesised VSG reaching the cell surface[7]. Here, we tested the effect of the hydrolytic enzymes in snake venom on the VSG coat.

Snake venoms are heterogeneous cocktails of proteins, including different snake venom metalloproteinases, snake venom serine proteinases, PLA_2s, three-finger toxins, and other minor components[26]. In particular, *Naja nigricollis* venom (NNV) was chosen as: (i) It is very active against cellular membranes in the eyes, the main target of venom being spat at a predator threatening a spitting cobra[27]. (ii) Cobras, such *N. nigricollis*, *N. katiensis*, *N. pallida,* and *N. nubiae,* have a significant proportion of PLA_2s in their venom compositions (20 to 30%). (iii) Unlike many other venoms, NNV composition has been characterised[17], and (iv) *N. nigricollis* PLA_2s have been structurally[15] and functionally[28] characterised. In this study, we observed that the effects of the PLA_2-enriched fraction 19 from NNV on trypanosomes can be blocked by the inhibitor *p*-bromophenacyl bromide, which has been extensively used to covalently modify the catalytic His-47 in PLA_2s and ultimately alter their tertiary structure[29]. This provides strong evidence that PLA_2s are the NNV components causing flagellar pocket enlargement and subsequent cell death.

Snake venom PLA_2s have evolved to attack plasma membrane components, and it was originally expected that a hydrolytic effect would have been observed on the GPI-anchor of VSG. However, the VSG, or at least GPI-anchored GFP, was unaffected by addition of exogenous PLA_2s, and instead a phenotype associated with disruption of endocytosis was observed. The observation that the effects of the PLA_2-enriched fraction 19 on trypanosomes can be blocked by the inhibitor *p*-bromophenacyl bromide further provided strong evidence that PLA_2s are the NNV components causing flagellar pocket enlargement and subsequent cell death. The mechanistic cause of the enlargement of the flagellar pocket remains unclear. The enlargement is not dependent on new protein synthesis, and this suggests a blockade in endocytosis, as reported for RNAi suppression of the clathrin light chain[8] or actin[18]. There was little effect on internal membrane compartments as judged by tagging various markers of internal compartments of the endosomal pathway. The exception was a change in the distribution of Rab11, which marks recycling vesicles[9]. This could be secondary as, if no endocytosis is occurring, there is nothing to recycle.

The cell cycle was disrupted by NNV addition. There was an abnormal proportion of cells showing two kinetoplasts and a twofold increase in cells with two flagellar pockets. These observations suggest an arrest in, or cells taking longer time than usual to traverse, the latter stages of the cell cycle. RNA interference of VSG mRNA causes an arrest in the early stages of cytokinesis possibly due to a shortage of new VSG-coated plasma membrane[30], and the effect of NNV may also reflect a plasma membrane defect. In cells with two flagellar pockets, only one of the pockets is enlarged by NNV, possibly reflecting a lack of activity on the new pocket.

The target for the toxic components causing flagellar pocket impairment and arrest of endocytosis remains to be elucidated. Trypanosomes perform clathrin-mediated endocytosis in the flagellar pocket. Endocytosis is a 2-step process. First, it is essential that the cargo gains access to the pocket through the flagellar pocket neck region. Second, the cargo can be endocytosed. This process is tightly controlled and includes a number of steps from vesicle budding to cargo selection, coat assembly, scission, and uncoating[31]. The pathway is regulated by the presence of phosphoinositides concentrated at the flagellar pocket[32]. TbPIPKA, a PIP kinase enzyme, is located at the neck of the flagellar pocket, the gate to the pocket, and involved in the first step in endocytosis. It has been described that depletion of TbPIPKA leads to an absence of phosphatidylinositol in the pocket, pocket enlargement, and arrest of endocytosis[33]. Extensive experiments would need to be performed to investigate whether TbPIPKA is the target for the toxic component. In the light of the current data, it is relevant to mention that when arrest of endocytosis occurs, there is no accumulation of AF-568-transferrin in the flagellar pocket. This observation points out two aspects. First, transferrin cannot penetrate though the flagellar pocket neck, indicating that arrest of endocytosis occurs in the first step of the process, just before penetration into the pocket lumen. Second, the enlargement may come from cargo being exported to the membrane or simply exocytosed. This would fit with the observations made from the experiments with CHX and NNV, where the phenotype is less pronounced than for NNV-only treatment. If protein synthesis is inhibited, less membrane molecules would be exported to the cell surface. Thus, evidence suggests that the target might be at the flagellar pocket neck, but further experiments should be performed to confirm this hypothesis.

Venoms have been used in the past as molecular tools for the study of trypanosomatid-related diseases[11–13]. However, the mechanisms leading to trypanocidal effects have never been characterised. Our work constitutes the first morphological and mechanistic description of the toxicity that seems to be triggered by *N. nigricollis* PLA_2s in *T. brucei*. We provide a description of a novel mechanism by which trypanosomes die. *N. nigricollis* PLA_2s likely cause cargo accumulation at the flagellar pocket, thus blocking endocytosis, a high-rate constitutive process for the cell, which is essential for parasite survival through immune evasion. Targeting trafficking pathways has been suggested as a potential alternative to improve treatment of Human African Trypanosomiasis[34]. While we remain skeptical that snake PLA_2s could serve as novel drug leads, the data presented in this study shine light on novel mechanisms for targeting and killing trypanosomes, which could potentially be exploited therapeutically.

Materials and methods

Snake venom. *Naja nigricollis* venom (NNV) from Tanzanian specimens was purchased in lyophilised form from Latoxan, France (cn. L1327B). Venom was reconstituted in HMI-9 media without fetal calf serum (FCS) when used in trypanosome cell culture.

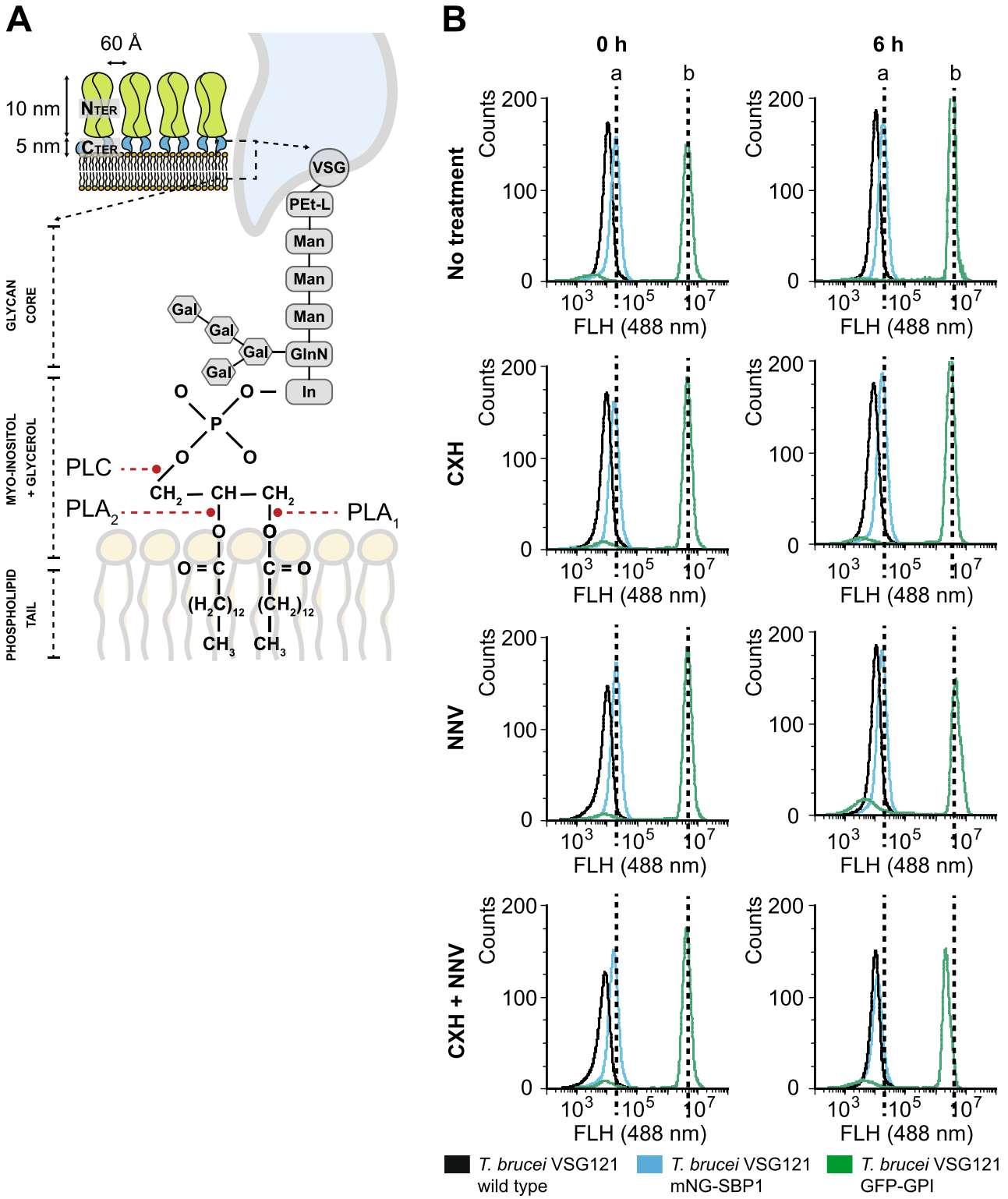
A
60 Å
10 nm
5 nm
NTER
CTER
VSG
PEt-L
Man
Man
Man
Gal
Gal
Gal
Gal
GlnN
In
GLYCAN CORE
MYO-INOSITOL + GLYCEROL
PHOSPHOLIPID TAIL
PLC
PLA2
PLA1
B
0 h
6 h
a
b
No treatment
CXH
NNV
CXH + NNV
Counts
FLH (488 nm)
T. brucei VSG121 wild type
T. brucei VSG121 mNG-SBP1
T. brucei VSG121 GFP-GPI

◂**Figure 5.** PLA_2 action is not sufficient to release GPI-anchored proteins. (**A**) Schematic representation of the GPI-anchor linking VSG C-terminus to the plasma membrane. The GPI anchor binds an aspartic acid from the VSG structure by a polyethylene glycol linker. This connects to a glycan core (three mannoses and one glucosamine branch linked to four galactoses). The glucosamine is bound to myo-inositol, which connects to the phospholipid tails. The sn2 acyl bond is the canonical target for PLA_2s, whereas PLA_1s hydrolyse 1-acyl bonds. *T. brucei* PLC is known to hydrolyse phosphate bonds linking myo-inositol to glycerol. (**B**) Live flow cytometry on *T. brucei* BSF VSG121 wild type (black), *T. brucei* BSF VSG121 mNG-SBP1 (blue), and *T. brucei* BSF VSG121 GFP-GPI (green). *T. brucei* BSF VSG121 wild type display 10^3 FAU due to its own autofluorescence. NNV (rich in PLA_2s) does not lead to a loss of fluorescence by hydrolysing GFP-GPI from the cell surface. In contrast, it allows a redistribution effect: Due to the hydrodynamic forces originating from the cell swimming, GFP-GPI is relocated to the flagellar pocket. There, endocytosis is blocked likely due to the PLA_2 blockade effect and, thus, GFP-GPI accumulates. There is not a significant loss of fluorescence, but a relocation from the cell surface to the flagellar pocket. Blocking protein synthesis (CHX) in combination to NNV leads to a reduction in the total fluorescence intensity as (i) there is no GFP-GPI being transported to the cell surface, and (ii) the GFP-GPI in the cell surface is being relocated to the flagellar pocket. In summary, these observations underpin the hypothesis that trypanocidal effect is likely caused by the ablation of endocytosis by PLA_2 action, enhanced by protein redistribution to the flagellar pocket, and not GPI hydrolysis.

Venom fractionation and proteomics characterisation. Whole venom fractionation was performed by reversed-phase high performance liquid chromatography (RP-HPLC) (Agilent 1200) on a C18 column (250 × 4.6 mm, 5 µm particle; Teknokroma), using HPLC Chromeleon software[35]. 2 mg/mL whole venom in phosphate-buffered saline (PBS: 137 mM NaCl, 3 mM KCl, 8 mM $Na_2HPO_4.2H_2O$, 1.4 mM KH_2PO_4) was loaded onto the column and run through an acetonitrile/trifluoracetic acid gradient for elution. Then solvent was evaporated using a speedvac. Finally, equivalent fractions from different rounds were pooled together in HMI-9 media without FCS. Fraction were analysed by SDS-PAGE (7%) and silver stained[36].

20 µg of fraction 19 were reduced with 5 mM Tris(2-carboxyethyl)phosphine (646,547, Sigma Aldrich) for 60 min at 65 °C, and afterwards alkylated with 20 mM 2-chloroacetamide (C0267, Sigma Aldrich) for 30 min at 65 °C. Proteins were digested with trypsin (V5280, Promega) overnight, with a trypsin:protein ratio of 1:50. Desalting was performed with in-house packed C18 disk tips following standard reversed-phase SPE protocols for sample cleanup[37,38]. LC–MS analysis was performed with 300 ng of sample injected in a Q Exactive hybrid quadrupole-Orbitrap mass spectrometer (Thermo Scientific), using an EASY-nLC 1200 System (LC140, ThermoFisher Scientific), and an EASY-Spray column (50 cm × 75 µm ID, PepMap RSLC C18, 2 µm ES803, Thermo Scientific), with a 70 min gradient length of increasing acetonitrile percentage. The mass spectrometer was operated in data dependent acquisition mode, scan range of 300–1750 m/z with MS resolution of 70,000, AGC target of 3e6 and maximum injection time of 20 ms. MS2 scans were obtained for top 10 precursors, with first mass of 120 m/z, resolution of 17,500, AGC target of 1×10^6, maximum injection time of 60 ms, 1.6 m/z isolation window, and NCE of 25.

Data analysis was conducted with Proteome Discoverer 2.4 (Thermo Scientific), with workflows adjusted for label free quantification. The FASTA database used was extracted from the reviewed snake venom protein list from the UniProt database (taxonomy: "Serpentes (snakes) [8570]" annotation: (type: "tissue specificity" venom) AND reviewed:yes) containing 2,330 venom proteins. Full digestion with trypsin was indicated in the settings, with two maximum missed cleavages allowed, and peptide length of 6–144. Precursor mass tolerance and fragment mass tolerance were set to 10 ppm and 0.02 Da, respectively. Oxidation (methionine) and deamidation (glutamine and asparagine), and acetylation (protein N-terminus) were added as variable modifications, while carbamidomethylation (cysteine) was added as static modification. Summed peptide area abundances were used to calculate master protein abundance (i.e. the protein chosen to represent the group in the cases where peptides identified match to multiple proteins), with filtering only for high confidence peptides (FDR 0.01). Data interpretation, processing, and plot generation were performed in Python 3.6 programming language.

Trypanosome cell culture. *T. brucei* Lister 427 VSG121 BSF cells were maintained in culture at a density of 1×10^5 to 2×10^6 cells/mL in HMI-9 supplemented with 10% (v/v) heat-inactivated FCS, penicillin (100 U/mL), and streptomycin (10 µg/mL), and kept at 37 °C and 5% CO_2. Cell counts were carried out using a hemocytometer.

Cell line engineering. A strategy using long oligonucleotide primers was used to tag endocytic pathway components[39]. In brief, forward primers contained the last 80 base pairs of the 5′ UTR of the target gene and the 20 base pairs of the 5′ pPOTv7 primer binding sequence; reverse primers contained the 20 base pairs of the 3′ pPOTv7 primer binding sequence and the first 80 base pairs of the target gene including the start codon, in the reverse complement[39]. PCR amplification from the pPOTv7 plasmid used resulted in a product carrying blasticidin resistance and mNEON green (mNG) protein. The 5′ UTR sequences were obtained from the TREU 927 reference genome for Tb927.10.12960 (Rab5A), Tb927.11.4570 (Rab5B), Tb927.8.4620 (Rab7), and Tb927.8.4330 (Rab11). PCR products were introduced into *T. brucei* Lister 427 expressing VSG221 by standard procedure, and transformants were selected with 10 µg/mL of blasticidin. Expected localisation of N-terminally tagged endocytic pathway proteins was confirmed by fluorescence microscopy. Following the same method, a *T. brucei* BSF Lister 427 cell line expressing VSG121 mNG-SBP1 was developed by C-terminally tagging SBP1 (Tb927.9.1970) with mNG. Successful tagging was confirmed by fluorescence microscopy.

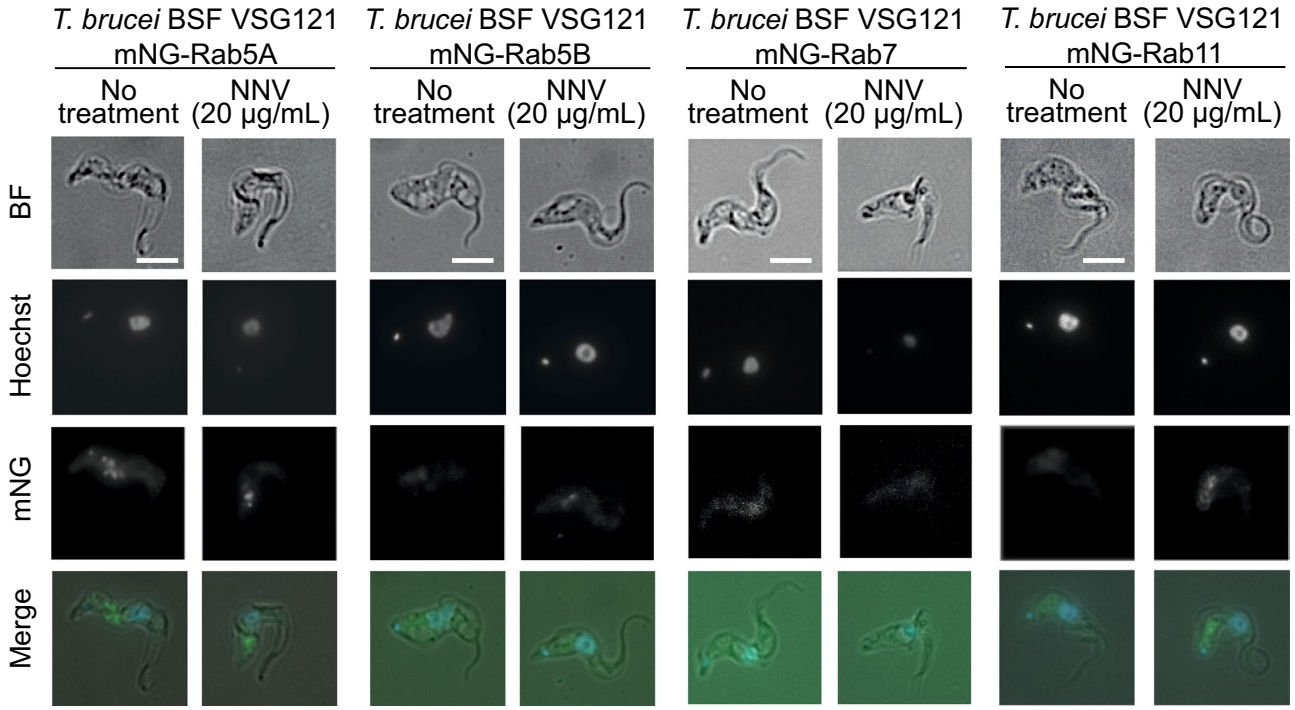

Figure 6. The downstream Rab11+ recycling endosome is likely affected by PLA_2 action. Fixed fluorescence microscopy (100X) was performed at 6 h post-NNV addition and no treatment conditions. 100 cells were observed per experiment (N = 3). Examples of representative cells shown in this figure. Rab5A+/5B+ and Rab7+ compartments remain unaffected, whereas the Rab11+ recycling endosome displayed a discrete and bright spot pattern as opposed to a more disperse one (no treatment). This provides an indication of the downstream consequences of the PLA_2 effects. Due to cargo accumulation at the flagellar pocket, the recycling endosome struggles to deliver recycled cargo back to the flagellar pocket, and its morphology is observably altered. Scale bar = 5 µm.

The *T. brucei* Lister 427 cell line expressing VSG121 GFP-GPI was engineered by introducing a transgene into the VSG121 expression site using the same approach as used to insert a second VSG[40] The plasmid p4716 was cut with Acc65I and SacI to release the insert, which was then used for transfections. The sequence of the insert is available in Fig. S1.

Cell morphology analysis. The morphology of all cell lines was analysed by fluorescence microscopy using Zeiss Axioimager M1. Images were processed using Zeiss AxioVision v5.6.1, analysed by NIH Image J, and made into figures in Adobe Illustrator.

For live cell microscopy, cells were incubated with 20 µg/mL of NNV, and 1 mL of cells was harvested at 3 and 6 h post-NNV addition. The sample was centrifuged for 1 min at 3000 rpm in an Eppendorf microfuge, the supernatant was removed, and the pellet was resuspended in 10 µL HMI-9. 4 µL were pipetted onto the microscope slide and covered by a 25 × 50 mm coverslip for visualisation. Untreated cell cultures were analysed alongside as negative control. For fixed cell microscopy, the procedure was identical, but 1% formaldehyde was added to the 10 µL resuspended cell pellet prior preparing the slide. Confocal microscopy was performed on live cells using the same method described above. Both the 2-dimensional images and the Z-stacks were processed by NIH Image J.

Cell cycle analysis. 1 mL of cells was harvested from the trypanosome culture and recovered by centrifugation at 10,000 rpm for 1 min. The supernatant was removed, 10 µL of HMI-9 was added, and the pellet was resuspended. 4% (w/v) paraformaldehyde was added to fix the cells. Finally, 1/100,000 Hoechst 33,342 was added. Fluorescence microscopy was then performed to visualise kinetoplast and nuclei in the cells.

Cell surface analysis. Cell surface fluorescence levels due to GFP-GPI were analysed by flow cytometry using a CytoFlex Flow Cytometer (Dept. of Pathology, University of Cambridge). *T. brucei* Lister 427 VSG121 (wild type) and *T. brucei* Lister 427 VSG121 p4716 (GFP-GPI) cells were incubated with 20 µg/mL NNV, and 1 mL of the cells was taken at 3 and 6 h post-NNV addition and transferred to a capped glass tube. Cells not subjected to NNV were also analysed in parallel. Wild type cells were used as a negative control for GFP fluorescence. The cytometer was set to record 10,000 events at 60 µL/min sample intake. A blank sample (pure water) was run between samples to avoid cell carry overs. The gating strategy employed aimed at separating single live cells from those dividing, forming clumps while dying, and debris. Data analysis was done using FlowJo software, and image processing was done in Adobe Illustrator.

AF-568-transferrin uptake assay. Endocytosis fitness was studied by performing an AF-568-transferrin uptake assays on live *T. brucei* Lister 427 VSG121 p4716 (GFP-GPI) cells. Bovine transferrin (Thermo Scientific #11107018) was first 2× dialysed in 1× PBS, and then fluorescently labeled with AF-568 using an Alexa Fluor™ 568 Protein Labeling Kit (Thermo Scientific #A10238), following the manufacturer's instructions. Cells were incubated for 12 h with 20 µg/mL NNV. At 0, 0.5, 1.5, and 6 h, 1 mL samples were taken, accounting for 3×10^5 cells. Each sample was spun down at 7,000 rpm for 2 min, washed in fresh HMI-9 media without serum, and resuspended in 100 µL + 1% BSA + 2 µL 2 mM FMK24 (Mu-Phe-hPhe-FMK, Sigma #M4070), a lysosomal protease inhibitor. The sample was incubated at room temperature for 5 min. Then, 80 nM AF-568-transferrin was added to the sample and incubated at 37 °C for 1 h. Last, the sample was centrifuged at 7,000 rpm for 2 min, and the cell pellet was resuspended in 20 µL HMI-9 without serum + 4% formaldehyde + 1/10,000 Hoechst 33342. The sample was incubated at room temperature for 10 min and then visualised by fluorescence microscopy.

SDS-PAGE and immunoblotting. Cell lysates were made by harvesting BSF cell culture. After centrifugation (3000 rpm, 10 min), the pellet was resuspended in 1 mL HMI-9 without serum and transferred into a 1.5 mL tube. The sample was centrifuged (10,000 rpm, 1 min), the supernatant was pipetted out. This step was repeated twice. Finally, the pellet was resuspended in HMI-9 + 1X SDS-PAGE sample buffer to a concentration of 10^8 cell equivalents/mL and incubated at 95 °C for 5 min. Then, SDS-PAGE was carried out[41]. For each sample, 10 µL of cell lysate (2×10^6 cell equivalents/well) was used. Gels were stained with Coomassie, silver staining[36], or transferred to a membrane. Immunoblotting was carried out as previously described[42]. Gel analysis was performed by NIH Image J, and the image was processed by Adobe Photoshop.

In vitro trypanosome cell killing assays. All cell lines were incubated with 20 µg/mL *N. nigricollis* whole venom (NNV) or with the relative concentration of each individual venom fraction. Trypanosome cell concentration at the start of the experiment was 1.5×10^5 cells/mL. Growth was measured by counting cells on a hemocytometer. Negative controls were carried out for all cell lines under conditions not containing NNV. The assays were performed in triplicates and collected data were Log_{10} transformed.

Protein synthesis inhibition assay. *T. brucei* Lister 427 VSG121 (wild type) and *T. brucei* Lister 427 VSG121 GFP-GPI cell lines were incubated with (i) 50 µg/mL cycloheximide (CHX); (ii) 20 µg/mL NNV; (iii) 50 µg/mL CHX + 20 µg/mL NNV; or (iv) HMI-9 media only. NNV was added one hour post CHX addition. Trypanosome cell concentration at the start of the experiments was 1.5×10^5 cells/mL. Growth was measured by counting cells on a hemocytometer at 1, 4, and 7 h post CHX addition. In addition, cell surface fluorescence was analysed by flow cytometry, and total GFP within the cell was analysed by anti-GFP western blot.

Received: 12 November 2021; Accepted: 25 March 2022
Published online: 16 April 2022

References

1. Buscher, P., Cecchi, G., Jamonneau, V. & Priotto, G. Human African trypanosomiasis. *Lancet* **390**(10110), 2397–2409. https://doi.org/10.1016/s0140-6736(17)31510-6 (2017).
2. Grunfelder, C. G. *et al.* Accumulation of a GPI-anchored protein at the cell surface requires sorting at multiple intracellular levels. *Traffic* **3**(8), 547–559. https://doi.org/10.1034/j.1600-0854.2002.30805.x (2002).
3. Overath, P. & Engstler, M. Endocytosis, membrane recycling and sorting of GPI-anchored proteins: *Trypanosoma brucei* as a model system. *Mol. Microbiol.* **53**(3), 735–744. https://doi.org/10.1111/j.1365-2958.2004.04224.x (2004).
4. Engstler, M. *et al.* Hydrodynamic flow-mediated protein sorting on the cell surface of trypanosomes. *Cell* **131**(3), 505–515. https://doi.org/10.1016/j.cell.2007.08.046 (2007).
5. Halliday, C. *et al.* trypanosomatid flagellar pocket: From structure to function. *Trends Parasitol.* **37**(4), 317–329. https://doi.org/10.1016/j.pt.2020.11.005 (2021).
6. Landfear, S. M. & Ignatushchenko, M. The flagellum and flagellar pocket of trypanosomatids. *Mol. Biochem. Parasitol.* **115**(1), 1–17. https://doi.org/10.1016/s0166-6851(01)00262-6 (2001).
7. Engstler, M. *et al.* Kinetics of endocytosis and recycling of the GPI-anchored variant surface glycoprotein in *Trypanosoma brucei*. *J. Cell Sci.* **117**(7), 1105–1115. https://doi.org/10.1242/jcs.00938 (2004).
8. Allen, C. L., Goulding, D. & Field, M. C. Clathrin-mediated endocytosis is essential in *Trypanosoma brucei*. *Embo J.* **22**(19), 4991–5002. https://doi.org/10.1093/emboj/cdg481 (2003).
9. Umaer, K., Bush, P. J. & Bangs, J. D. Rab11 Mediates selective recycling and endocytic trafficking in *Trypanosoma brucei*. *Traffic* **19**(6), 406–420. https://doi.org/10.1111/tra.12565 (2018).
10. Link, F., Borges, A. R., Jones, N. G. & Engstler, M. To the surface and back: Exo- and endocytic pathways in *Trypanosoma brucei*. *Front. Cell Dev. Biol.* **9**, 15. https://doi.org/10.3389/fcell.2021.720521 (2021).
11. Boutrin, M. C. F., Foster, H. A. & Pentreath, V. W. The effects of bee (*Apis mellifera*) venom phospholipase A_2 on *Trypanosoma brucei* brucei and enterobacteria. *Exp. Parasitol.* **119**(2), 246–251. https://doi.org/10.1016/j.exppara.2008.02.002 (2008).
12. Nunes, D. C. O. *et al.* BnSP-7 Toxin, a basic phospholipase A_2 from *Bothrops pauloensis* snake venom interferes with proliferation, ultrastructure and infectivity of *Leishmania amazonensis*. *Parasitology* **140**(7), 844–854. https://doi.org/10.1017/s0031182013000012 (2013).
13. de Moura, A. A. *et al.* Purification and biochemical characterization of three myotoxins from bothrops mattogrossensis snake venom with toxicity against leishmania and tumor cells. *Biomed. Res. Int.* **2014**, 13. https://doi.org/10.1155/2014/195356 (2014).
14. Davidson, F. F. & Dennis, E. A. Evolutionary relationships and implications for the regulation of phospholipase A_2 from snake venom to human secreted forms. *J. Mol. Evol.* **31**(3), 228–238. https://doi.org/10.1007/bf02109500 (1990).
15. Kini, R. M. & Evans, H. J. The role of enzymatic activity in inhibition of the extrinsic tenase complex by phospholipase A_2 isoenzymes from *Naja nigricollis* venom. *Toxicon* **33**(12), 1585–1590. https://doi.org/10.1016/0041-0101(95)00103-4 (1995).

16. Kini, R. M. Excitement ahead: Structure, function and mechanism of snake venom phospholipase A_2 enzymes. *Toxicon* **42**(8), 827–840. https://doi.org/10.1016/j.toxicon.2003.11.002 (2003).
17. Petras, D. *et al.* Snake venomics of African spitting cobras: Toxin composition and assessment of congeneric cross-reactivity of the pan-African EchiTAb-Plus-ICP antivenom by antivenomics and neutralization approaches. *J. Proteome Res.* **10**(3), 1266–1280. https://doi.org/10.1021/pr101040f (2011).
18. Garcia-Salcedo, J. A. *et al.* a differential role for actin during the life cycle of *Trypanosoma brucei*. *Embo J.* **23**(4), 780–789. https://doi.org/10.1038/sj.emboj.7600094 (2004).
19. Mora-Obando, D., Díaz, C., Angulo, Y., Gutiérrez, J. M. & Lomonte, B. Role of enzymatic activity in muscle damage and cytotoxicity induced by *Bothrops asper* Asp49 phospholipase A_2 myotoxins: Are there additional effector mechanisms involved? *PeerJ* **2**, e569. https://doi.org/10.7717/peerj.569 (2014).
20. Shaner, N. C. *et al.* A bright monomeric green fluorescent protein derived from *Branchiostoma lanceolatum*. *Nat. Methods.* **10**(5), 407–409. https://doi.org/10.1038/nmeth.2413 (2013).
21. Dean, S., Sunter, J. D. & Wheeler, R. J. TrypTag.org: A trypanosome genome-wide protein localisation resource. *Trends Parasitol.* **33**(2), 80–82. https://doi.org/10.1016/j.pt.2016.10.009 (2016).
22. Dong, X., Lim, T. K., Lin, Q. & He, C. Y. Basal body protein TbSAF1 is required for microtubule quartet anchorage to the basal bodies in *Trypanosoma brucei*. *MBio* **11**(3), e00668–e00720. https://doi.org/10.1128/mBio.00668-20 (2020).
23. Seiser, R. M. & Nicchitta, C. V. The fate of membrane-bound ribosomes following the termination of protein synthesis. *J. Biol. Chem.* **275**(43), 33820–33827. https://doi.org/10.1074/jbc.M004462200 (2000).
24. Vanhollebeke, B., Uzureau, P., Monteyne, D., Pérez-Morga, D. & Pays, E. Cellular and molecular remodeling of the endocytic pathway during differentiation of trypanosoma brucei bloodstream forms. *Eukaryot. Cell.* **9**(8), 1272–1282. https://doi.org/10.1128/EC.00076-10 (2010).
25. Field, M. C., Natesan, S. K. A., Gabernet-Castello, C. & Koumandou, V. L. Intracellular trafficking in the trypanosomatids. *Traffic* **8**(6), 629–639. https://doi.org/10.1111/j.1600-0854.2007.00558.x (2007).
26. Laustsen, A. H. *et al.* From fangs to pharmacology: The future of snakebite envenoming therapy. *Curr. Pharm. Des.* **22**(34), 5270–5293. https://doi.org/10.2174/1381612822666160623073438 (2016).
27. Chang, K. C. *et al.* Venom ophthalmia and ocular complications caused by snake venom. *Toxins.* **12**(9), 15. https://doi.org/10.3390/toxins12090576 (2020).
28. Kerns, R. T., Kini, R. M., Stefansson, S. & Evans, H. J. Targeting of venom phospholipases: The strongly anticoagulant phospholipase A_2 from *Naja nigricollis* venom binds to coagulation factor X_a to inhibit the prothrombinase complex. *Arch. Biochem. Biophys.* **369**(1), 107–113. https://doi.org/10.1006/abbi.1999.1345 (1999).
29. Tatulian, S. A. Structural effects of covalent inhibition of phospholipase A_2 suggest allosteric coupling between membrane binding and catalytic sites. *Biophys. J.* **84**(3), 1773–1783. https://doi.org/10.1016/S0006-3495(03)74985-6 (2003).
30. Sheader, K. *et al.* Variant surface glycoprotein RNA interference triggers a precytokinesis cell cycle arrest in African trypanosomes. *Proc. Natl. Acad. Sci. U.S.A.* **102**(24), 8716–8721. https://doi.org/10.1073/pnas.0501886102 (2005).
31. McMahon, H. T. & Boucrot, E. Molecular mechanism and physiological functions of clathrin-mediated endocytosis. *Nat. Rev. Mol. Cell Biol.* **12**(8), 517–533. https://doi.org/10.1038/nrm3151 (2011).
32. Manna, P. T. & Field, M. C. Phosphoinositides, kinases and adaptors coordinating endocytosis in *Trypanosoma brucei*. *Commun. Integr. Biol.* **8**(6), e1082691. https://doi.org/10.1080/19420889.2015.1082691 (2015).
33. Demmel, L. *et al.* The endocytic activity of the flagellar pocket in *Trypanosoma brucei* is regulated by an adjacent phosphatidylinositol phosphate kinase. *J Cell Sci.* **129**(11), 2285–2285. https://doi.org/10.1242/jcs.191569 (2016).
34. Quintana, J. F., Pino, R. C. D., Yamada, K. & Zhang, N. Adaptation and therapeutic exploitation of the plasma membrane of African trypanosomes. *Genes* **9**(7), 368. https://doi.org/10.3390/genes9070368 (2018).
35. Ahmadi, S. *et al.* An in vitro methodology for discovering broadly-neutralizing monoclonal antibodies. *Sci. Rep.* **10**(1), 7. https://doi.org/10.1038/s41598-020-67654-7 (2020).
36. Chevallet, M., Luche, S. & Rabilloud, T. Silver staining of proteins in polyacrylamide gels. *Nat. Protoc.* **1**(4), 1852–1858. https://doi.org/10.1038/nprot.2006.288 (2006).
37. Poole, C. F. New trends in solid-phase extraction. *Trac-Trends Anal. Chem.* **22**(6), 362–373. https://doi.org/10.1016/s0165-9936(03)00605-8 (2003).
38. Tubaon, R. M., Haddad, P. R. & Quirino, J. P. Sample clean-up strategies for ESI mass spectrometry applications in bottom-up proteomics: Trends from 2012 to 2016. *Proteomics* **17**(20), 1700011. https://doi.org/10.1002/pmic.201700011 (2017).
39. Dean, S. *et al.* A toolkit enabling efficient, scalable and reproducible gene tagging in trypanosomatids. *Open Biol.* **5**(1), 12. https://doi.org/10.1098/rsob.140197 (2015).
40. Maudlin, I. E., Kelly, S., Schwede, A. & Carrington, M. VSG mRNA levels are regulated by the production of functional VSG protein. *Mol. Biochem. Parasitol.* **241**, 7. https://doi.org/10.1016/j.molbiopara.2020.111348 (2021).
41. Walker, J. M. SDS polyacrylamide gel electrophoresis of proteins. In *The Protein Protocols Handbook* (ed. Walker, J. M.) 177–185 (Humana Press Inc, 2009).
42. Hnasko, T. S. & Hnasko, R. M. The western blot. In *ELISA: Methods and Protocols* Vol. 1318 (ed. Hnasko, R.) 87–96 (Humana Press Inc, 2015).

Acknowledgements

We thank Dr. Sam Dean for kindly providing the plasmid pPOTv7. MC is a Wellcome Investigator (217138/Z/19/Z). We thank Wellcome for the funding for this study.

Author contributions

A.M.E., M.C., and A.H.L. conceived the study. A.M.E., A.H.L, O.J.S.M., I.M., K.K. and J.A.J. performed and analysed the experiments. A.M.E., M.C., and A.H.L. wrote the manuscript. All authors contributed to editing the manuscript.

Competing interests

The authors declare no competing interests.

Additional information

Supplementary Information The online version contains supplementary material available at https://doi.org/10.1038/s41598-022-10091-5.

Correspondence and requests for materials should be addressed to A.H.L.